PROCEEDINGS OF SCIENCE

Energy density functional approaches to inhomogeneous superfluid neutron-star matter

Takashi Nakatsukasa[a,b,c,*] **and Chengpeng Yu**[a]

[a] *Center for Computational Sciences, University of Tsukuba*
Tsukuba 305-8577, Japan
[b] *Department of Physics, Institute for Pure and Applied Sciences, University of Tsukuba*
Tsukuba 305-8577, Japan
[c] *RIKEN Nishina Center*
Wako 351-0198, Japan
E-mail: nakatsukasa@nucl.ph.tsukuba.ac.jp,
yu.chengpeng@nucl.ph.tsukuba.ac.jp

We present recent developments in numerical methods for the energy density functional calculations, suitable for massively parallel computing: The Green's function with shifted Krylov subspace method and the Fermi operator expansion method. Some applications of those methods to inhomogeneous nuclear matter are presented. This may elucidate the transport properties of the superfluid neutrons in the inner crust of neutron stars, which are essential ingredients in pulsar glitch phenomena.

10th International Conference on Quarks and Nuclear Physics (QNP2024)
8-12 July, 2024
Barcelona, Spain

*Speaker

PoS(QNP2024)170

1. Introduction

A neutron star is an extremely dense and compact object in the universe. It is primarily a macroscopic nucleus with a radius of about 10 km, made of nucleons (neutrons and protons) together with leptons. Naturally, its structure and dynamics have been of great interest in nuclear physics. The central part of the neutron star with the highest density, called the inner core, may contain hyperons and possibly a quark matter. In contrast, a region near the surface is called the crust, where the nuclear matter is composed of nucleons, however, it has prominent inhomogeneous structures. The crust is roughly divided into two, outer and inner crusts. In the outer crust, neutron-rich nuclei build a Coulomb lattice, while the nuclei go beyond the neutron dripline and coexist with free neutrons in the inner crust. A variety of structures are predicted for the inner crust, including exotic ones such as the presence of deformed nuclei [1], and the pasta phases [2–4]. To cope with the emergence of various structures in the inner crust, we need computational approaches capable of studying three-dimensional (3D) non-uniform structure with unbound neutrons in the continuum.

The mean-field approaches, energy density functional methods in nuclear physics, have been playing a central role in studying heavy nuclei and nuclear matter [5, 6]. The static Hartree-Fock-Bogoliubov (HFB) calculation requires the self-consistency between the HFB (ground) state and the HFB Hamiltonian. A standard procedure for the HFB solutions is as follows [7].

1. Diagonalize the HFB Hamiltonian and obtain wave functions (U, V) for the quasiparticle-energy eigenstates.
2. Calculate the normal ρ and pair densities κ using the quasiparticle wave functions (U, V), then, determine the HFB Hamiltonian (potentials).
3. Go back to 1 and repeat the procedure until we reach the self-consistency between the Hamiltonian and the densities.

For the full 3D unrestricted calculations, finding a self-consistent solution demands successive diagonalization of matrices with large dimension N. Each diagonalization procedure computationally costs $O(N^3)$. Thus, most of the available codes of the HFB calculation utilize some symmetry restriction on the densities, such as spatial symmetry and time-reversal symmetry, in order to reduce both the matrix dimension and the number of iteration [8–10]. The HFB program HFODD [11] can perform unrestricted calculations for finite bound nuclei. However, it is impossible to calculate the inner crust because it uses the harmonic-oscillator-basis states which are unsuitable for a description of the free neutrons.

A new approach to the HFB solutions has been proposed in Ref. [12] and extended to the finite temperature [1]. One of the prominent features of these approaches is that these approaches do not calculate the quasiparticle wave functions, thus, do not require the diagonalization of the Hamiltonian matrix. Instead, they utilize the shifted Krylov subspace methods to calculate the Green's function $G(\mathbf{r}\sigma, \mathbf{r}'\sigma'; z)$ where z is the complex energy, over which the contour integration is performed to produce the densities, ρ and κ. It is suited for parallel computing because the Green's function $G(\mathbf{r}\sigma, \mathbf{r}'\sigma'; z)$ is calculable independently for each point $(\mathbf{r}', \sigma')$. At finite temperature, we need to subtract contributions at the Matsubara frequencies, for which Minimum computational cost is required with the shifted method [1]. This method is presented in Sec. 2.

Another approach, the Fermi operator expansion (FOE) method [13], was tested and adopted for the calculation of the non-uniform nuclear matter in Ref. [14]. In the FOE method, the Fermi-

Dirac distribution function is expanded in terms of polynomials. Then, the densities, ρ and κ, are constructed by multiplication of the mean-field Hamiltonian on adopted basis states. The method does not use matrix diagonalization and is suitable for parallel computing. In Sec. 3, we present this FOE method as an efficient solver for the finite-temperature HFB (FT-HFB) problems.

Transport properties of the free neutrons in the inner crust of neutron stars have been of great interest, linked to various phenomena observed in pulsars. In particular, one of the most impressive phenomena, the pulsar glitch, is supposed to take place in the inner crust. The neutron stars are observed as the pulsar that emits electromagnetic radiation with a regular interval. This interval can be regarded as a rotational period of the neutron star which gradually increases because it loses the angular momentum by the radiation. However, occasionally, we observe a sudden decrease in the rotational period, that is the pulsar giltch. The first pulsar glitch was observed about half a century ago, however, its origin and mechanism are still under debate. One of the unsolved questions is whether the inner crust can carry enough amount of angular momentum which is consistent with the magnitude of the observed glitch. The mobility of the free neutrons has a direct consequence on this issue. In Sec. 4, we discuss the transport properties of the free neutrons, such as the effective mass and effects of the superfluidity.

2. HFB Green's function with shifted Krylov subspace method

In the FT-HFB theory, the partition function for the grand canonical ensemble with the temperature T, the volume V, and the chemical potential μ is given by

$$Z_{\rm HFB}(T,V,\mu) = e^{-\beta(E_0-\mu N_0)} \prod_{k>0} \left(1+e^{\beta E_k}\right), \tag{1}$$

where E_0 is the energy of the HFB ground state $|0\rangle$ with the average particle number N_0. $k>0$ means the quasiparticle states with positive eigenenergies $E_k > 0$ of the HFB Hamiltonian $H_{\rm HFB}$ [7]. Using the density matrix operator $\hat\rho_{\rm HFB} \equiv e^{-\beta\hat H'}/Z_{\rm HFB}(T,V,\mu)$, where $\hat H' \equiv E_0 - \mu N_0 + \sum_{k>0} E_k a_k^\dagger a_k$ where $a_k^\dagger$ (a_k) are the quasiparticle creation (annihilation) operators, the normal one-body and the pair densities are given by

$$\rho(\xi,\xi') \equiv {\rm Tr}\left[\hat\rho_{\rm HFB}\hat\psi^\dagger(\xi')\hat\psi(\xi)\right], \qquad \kappa(\xi,\xi') \equiv {\rm Tr}\left[\hat\rho_{\rm HFB}\hat\psi(\xi')\hat\psi(\xi)\right], \tag{2}$$

where ξ represents the coordinate and spin, $(\mathbf{r},\sigma)$. The generalized density can be written as

$$\begin{aligned} R(\xi,\xi') &\equiv \begin{pmatrix} \rho(\xi,\xi') & \kappa(\xi,\xi') \\ -\kappa^*(\xi,\xi') & 1-\rho^*(\xi,\xi') \end{pmatrix} = {\rm Tr}\left[\begin{pmatrix} \hat\psi(\xi) \\ \hat\psi^\dagger(\xi) \end{pmatrix} \hat\rho_{\rm HFB} \begin{pmatrix} \hat\psi^\dagger(\xi') & \hat\psi(\xi') \end{pmatrix}\right], \\ &= \sum_{k\gtrless 0} \begin{pmatrix} U_k(\xi) \\ V_k(\xi) \end{pmatrix} f_T(E_k) \begin{pmatrix} U_k(\xi') \\ V_k(\xi') \end{pmatrix}^\dagger, \end{aligned} \tag{3}$$

where $f_T(x) = (1+e^{\beta x})^{-1}$ is the Fermi-Dirac function. $(U_k, V_k)^T$ are the quasiparticle wave functions with the eigenenergies E_k. The negative-energy solutions ($k<0$) can be obtained from the positive-energy ones ($k>0$) as

$$H_{\rm HFB}\begin{pmatrix} U_k \\ V_k \end{pmatrix} = E_k \begin{pmatrix} U_k \\ V_k \end{pmatrix}, \qquad \begin{pmatrix} U_{-k} \\ V_{-k} \end{pmatrix} = \begin{pmatrix} V_k^* \\ U_k^* \end{pmatrix}, \qquad E_{-k} = -E_k. \tag{4}$$

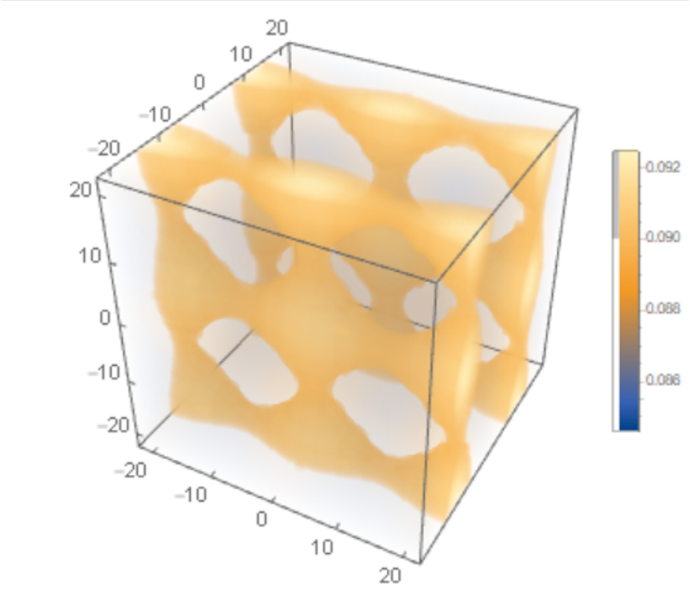

Figure 1: Beta-equilibrium state calculated with a box size of $(45\ \mathrm{fm})^3$ and the neutron chemical potential $\mu_n = 14$ MeV, at the temperature $k_B T = 200$ keV.

The Green's function (resolvent) $G(z)$ with a complex energy z is defined as a solution of the following equation.

$$(zI - H_{\mathrm{HFB}})\, G(z) = I. \tag{5}$$

We can prove that the generalized density can be obtained by performing the contour integration over a closed path C (boundary of a region S) on the complex energy plane [1].

$$R = \frac{1}{2\pi i} \oint_C f_T(z) G(z) \mathrm{d}z + \frac{1}{\beta} \sum_{i\omega_n \in S} G(i\omega_n), \tag{6}$$

where $i\omega_n \equiv i(2n+1)\pi/\beta$ are the Matsubara frequencies on the imaginary axis. The generalized density R contains all the necessary information to construct the HFB Hamiltonian.

The main computational task is to solve Eq. (5) for many complex energy z on the contour C and at the Matsubara frequencies $z = i\omega_n$. To achieve this, we use the shifted conjugate-orthogonal conjugate-residual (COCR) method [1]. The shifted algorithm allows us to obtain $G(z)$ simultaneously for different z values with a minimum effort, by iteratively solving Eq. (5) for a single value of z. The method is applied to liquid-gas and shape phase transitions in finite nuclei and the inner-crust structures of neutron stars [1].

The numerical calculation is performed with 3D coordinate mesh space with $\Delta x = \Delta y = \Delta z = 1$ fm assuming the periodic boundary condition for the 3D cubic box. With a given chemical potential for neutrons μ_n, the proton chemical potential is determined by the charge neutral and the beta equilibrium conditions, assuming the uniform electron density. Using the Skyrme energy density functional of SLy4, an equilibrium state with the face-centered configuration (fcc) is obtained at $\mu_n = 11$ MeV. In a 3D box of $(45\ \mathrm{fm})^3$ at the temperature $\beta^{-1} = 200$ keV, there are four deformed Se nuclei with 136 protons and about 4,000 superfluid neutrons. This is shown in Ref. [1]. Increasing the neutron chemical potential to $\mu_n = 14$ MeV, a completely different structure emerges, which is

shown in Fig. 1. The fcc structure is destroyed and the slab nuclei with holes appear. Since the box size is not optimized, we cannot say that these exotic phases exist in the inner crust. Nevertheless, the calculation suggests that unknown structures may appear in the crust region, implying the importance of the 3D unrestricted calculations.

3. Fermi operator expansion (FOE) method

The generalized density of Eq. (3) can be rewritten as

$$R = \sum_{k\gtrless 0} \begin{pmatrix} U_k \\ V_k \end{pmatrix} f_T(E_k) \begin{pmatrix} U_k \\ V_k \end{pmatrix}^\dagger = f_T(H_{\rm HFB}) \sum_{k\gtrless 0} \begin{pmatrix} U_k \\ V_k \end{pmatrix} \begin{pmatrix} U_k \\ V_k \end{pmatrix}^\dagger = f_T(H_{\rm HFB}). \tag{7}$$

Here, we use the completeness relation

$$\begin{pmatrix} U_k \\ V_k \end{pmatrix} \begin{pmatrix} U_k \\ V_k \end{pmatrix}^\dagger = I, \qquad I\text{: Identity matrix} \tag{8}$$

Therefore, the generalized density matrix is identical to the Fermi-Dirac function $f_T(x)$ whose argument x is replaced by the HFB Hamiltonian matrix $H_{\rm HFB}$.

The FOE method utilizes a polynomial expansion for the Fermi-Dirac function $f_T(x)$ in the section $x_{\rm min} < x < x_{\rm max}$. Here, we use the Chebyshev polynomials $T_n(y)$ $(n = 0, 1, \cdots)$, where $y = (x - x_+)/x_-$ with $x_\pm = (x_{\rm max} \pm x_{\rm min})/2$. Note that the Chebyshev polynomials $T_n(y)$ are defined in the section of $-1 < y < 1$.

$$f_T(x) = f_T(x_+ + x_- y) \approx \sum_{n=0}^{M} \frac{a_n}{1+\delta_{n0}} T_n(y), \tag{9}$$

where M is the maximum degree. Since the function $f_T(x)$ approaches to the step function $\theta(-x)$ at the $T = 0$ limit, a larger value of M is required for a lower temperature. In the present case, we expand the Fermi-Dirac operator on the right-hand side of Eq. (7), that can be done by replacing the variable x in Eq. (9) by $H_{\rm HFB}$. The upper (lower) limits of the argument are given by the maximum (minimum) quasiparticle energy, $x_{\rm max} = E_{\rm max}$ ($x_{\rm min} = E_{\rm min}$), in the adopted model space. Because of the symmetric property of the quasiparticle energies of Eq. (4), we should take $x_{\rm min} = -x_{\rm max}$.

The Chebyshev polynomials are orthogonal with respect to the weight of $1/\sqrt{1-x^2}$.

$$\int_{-1}^{1} T_n(x) T_m(x) \frac{dx}{\sqrt{1-x^2}} = N_n \delta_{nm}, \tag{10}$$

with the normalization constants $N_0 = \pi$ and $N_n = \pi/2$ $(n \neq 0)$. The coefficients in Eq. (9) are

$$a_n = \frac{2}{\pi} \int_{-1}^{1} T_n(y) f_T(x_+ + x_- y) \frac{dy}{\sqrt{1-y^2}}. \tag{11}$$

The factor of $(1+\delta_{n0})^{-1}$ in Eq. (9) is introduced to simplify the expression of Eq. (11).

The densities are calculated using the recursive relation for the Chebyshev polynomials:

$$T_{n+1}(y) = 2y T_n(y) - T_{n-1}(y), \quad n \geq 1. \tag{12}$$

Let us define the dimensionless Hamiltonian $H_y \equiv (H_{\rm HFB} - x_+)/x_-$ and $|j\rangle$ as a unit vector that the jth row in the HFB state $(U, V)^T$ is unity and all the others are zero. Starting from $|j_0\rangle = |j\rangle$ and $|j_1\rangle = H_y\,|j\rangle$, a series of the states are calculated using the recursive relation (12):

$$|j_{n+1}\rangle = 2H_y\,|j_n\rangle - |j_{n-1}\rangle\,, \quad n = 1, \cdots, M-1. \tag{13}$$

The matrix elements R_{ij} of Eq. (7) are calculated as

$$\langle i\,|\,R\,|\,j\rangle = \langle i\,|\,f_T(H_{\rm HFB})\,|\,j\rangle \approx \sum_{n=0}^{M} \frac{a_n}{1+\delta_{n0}}\,\langle i|j_n\rangle\,. \tag{14}$$

From this expression, it is obvious that the calculation can be easily parallelized by assigning the calculation of R_{ij} with different j to different processors, because one can independently compute $\langle i\,|\,R\,|\,j\rangle$ for each ket state $|j\rangle$ using Eqs. (13) and (14).

4. Pulsar glitches and transport properties of superfluid neutrons

The pulsar glitch has been regarded as a signature of the superfluid neutrons inside the neutron stars [15]. The rotational frequency of charged components, which are observed by the electromagnetic radiation, gradually becomes smaller in time. However, that of the superfluid neutrons remains the same as the vortices in the superfluid are pinned to the crust nuclei. Thus, the spin difference between these two components increases. At a threshold spin lag, the vortices are no longer pinned and their angular momenta are suddenly transferred to the crust, which is observed as the glitch [16]. This glitch scenario has many features superior to others, however, there remain some issues to be solved, such as the magnitude of the pinning interaction between the vortex and the nucleus, and the location of the superfluid where the angular momenta are stored. Let us discuss the second issue here. The most natural (promising) candidate for the glitch location is the inner crust, since both the crust nuclei and the superfluid neutrons are present. Then, the question is how much angular momentum can be stored in the superfluid neutrons of the inner crust. The answer requires the knowledge on transport properties of the superfluid neutrons. Especially, the nondissipative entrainment effects are known to provide a strong impact on the glitch scenario [17, 18]. In fact, Chamel [19] predicted that effective neutron mass m_n^* in the inner crust is significantly larger than the bare neutron mass m_n, which indicates the reduced mobility of the neutrons due to the Bragg scattering from the crust nuclei.

Let us assume that the charged (crust) component rotates with the rotational frequency Ω and the neutron superfluid does with Ω_n. A rotating two-component fluid model provides the ratio of moments of inertia, I_n/I, where I and I_n are those of the entire neutron star and the superfluid neutron component, respectively [17].

$$\frac{I_n}{I} \approx 2\tau_c \mathcal{A} \frac{\langle m_n^* \rangle}{m_n}, \qquad \text{where} \quad \mathcal{A} = \frac{1}{t_{\rm obs}} \left(\sum_i \frac{\Delta\Omega_i}{\Omega} \right) \tag{15}$$

where $\tau_c = -\Omega/(2\dot{\Omega})$ is the characteristic age of the pulsar which is observed as a change in the pulsar period. The quantity $\mathcal{A}$ can be determined by the glitch observation: $\Delta\Omega/\Omega$ is the relative magnitude of the glitch which are summed over several glitches during period $t_{\rm obs}$. The observation

data tell us that the superfluid neutrons in the inner crust are not enough to explain I_n/I in Eq. (15), if the average effective mass $\langle m_n^* \rangle$ is several times larger than the bare mass [17, 18]. The band calculation [19] seems to suggest a conflict with the observed glitch data in the present scenario.

To settle the problem, it is desirable to perform the self-consistent band calculation for the inner crust of neutron stars with modern EDFs. In Ref. [20], the "anti-entrainment" effect $\langle m_n^* \rangle / m_n < 1$ was suggested for the slab phase. In addition, there is an argument that the effect of the Bragg scattering would be hindered by the pairing (superfluidity) of the neutrons [21]. We show here a result of a simple potential model calculation to demonstrate the effect of the pairing. The potential is assumed to be a Woods-Saxon shape and the depth is taken as 50 MeV, which simulates that obtained by the self-consistent calculation for the slab phase at the baryon density $\rho_B = 0.07$ fm^{-3} [20]. The simple constant pairing gap Δ is adopted. The superfluid neutron ratio which is the inverse of the effective mass, $n_s/n = m_n/\langle m_n^* \rangle$ is shown in Fig. 2. The effective mass is large $\langle m_n^* \rangle / m_n \approx 3$ at $\Delta = 0$, while it is approximately unity $\langle m_n^* \rangle \approx m_n$ at $\Delta \gtrsim 1$ MeV. Although the calculation is still in the preliminary stage, this suggests the importance of the superfluidity for the accurate estimation of the effective mass.

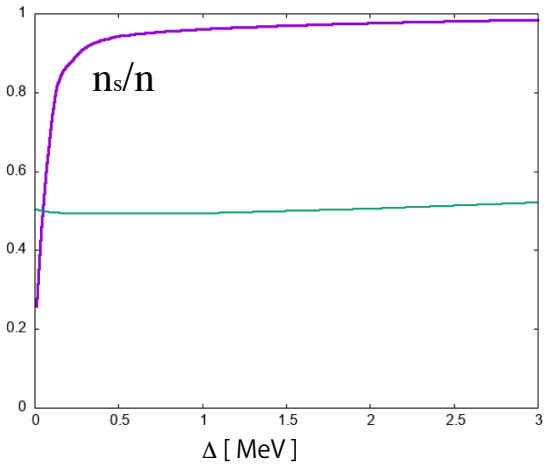

Figure 2: Superfluid ratio n_s/n for the system with $\mu_n = 3$ MeV for a one-dimensional potential model. The green line represents the ratio of neutrons in the unbound orbits to the entire neutrons. See text for details.

The full 3D self-consistent calculations with the band theory are highly desired to settle the controversial issues related to the pulsar gliches. Further developments and investigations toward this goal are under progress.

Acknowledgments

This work is supported in part by JSPS KAKENHI Grant No. JP23K25864, JST-ERATO Grant No. JPMJER2304, and by JSPS A3 Foresight Program No. JPJSA3F20190002. The computational resources are provided in part through the HPCI System Research Project (Project ID: hp200069), and by Multidisciplinary Cooperative Research Program in Center for Computational Sciences, University of Tsukuba.

References

[1] Y. Kashiwaba and T. Nakatsukasa, *Coordinate-space solver for finite-temperature Hartree-Fock-Bogoliubov calculations using the shifted Krylov method*, *Phys. Rev. C* **101** (2020) 045804.

[2] D.G. Ravenhall, C.J. Pethick and J.R. Wilson, *Structure of matter below nuclear saturation density*, *Phys. Rev. Lett.* **50** (1983) 2066.

[3] M. Hashimoto, H. Seki and M. Yamada, *Shape of nuclei in the crust of neutron star*, *Prog. Theor. Phys.* **71** (1984) 320.
[4] K. Oyamatsu, *Nuclear shapes in the inner crust of a neutron star*, *Nucl. Phys. A* **561** (1993) 431 .
[5] M. Bender, P.H. Heenen and P.-G. Reinhard, *Self-consistent mean-field models for nuclear structure*, *Rev. Mod. Phys.* **75** (2003) 121.
[6] T. Nakatsukasa, K. Matsuyanagi, M. Matsuo and K. Yabana, *Time-dependent density-functional description of nuclear dynamics*, *Rev. Mod. Phys.* **88** (2016) 045004.
[7] P. Ring and P. Schuck, *The nuclear many-body problems*, Texts and monographs in physics, Springer-Verlag, New York (1980).
[8] K. Bennaceur and J. Dobaczewski, *Coordinate-space solution of the Skyrme-Hartree-Fock Bogolyubov equations within spherical symmetry. the program HFBRAD (v1.00)*, *Comput. Phys. Comm.* **168** (2005) 96 .
[9] R.N. Perez, N. Schunck, R.-D. Lasseri, C. Zhang and J. Sarich, *Axially deformed solution of the Skyrme–Hartree–Fock–Bogolyubov equations using the transformed harmonic oscillator basis (iii) HFBTHO (v3.00): A new version of the program*, *Comput. Phys. Comm.* **220** (2017) 363 .
[10] W. Ryssens, V. Hellemans, M. Bender and P.-H. Heenen, *Solution of the Skyrme–HF+BCS equation on a 3d mesh, ii: A new version of the EV8 code*, *Comput. Phys. Comm.* **187** (2015) 175 .
[11] N. Schunck, J. Dobaczewski, W. Satuła, P. Bączyk, J. Dudek, Y. Gao et al., *Solution of the Skyrme-Hartree–Fock–Bogolyubov equations in the cartesian deformed harmonic-oscillator basis. (viii) HFODD (v2.73y): A new version of the program*, *Comput. Phys. Comm.* **216** (2017) 145 .
[12] S. Jin, A. Bulgac, K. Roche and G. Wlazłowski, *Coordinate-space solver for superfluid many-fermion systems with the shifted conjugate-orthogonal conjugate-gradient method*, *Phys. Rev. C* **95** (2017) 044302.
[13] S. Wu and C. Jayanthi, *Order-N methodologies and their applications*, *Phys. Rep.* **358** (2002) 1.
[14] T. Nakatsukasa, *Fermi operator expansion method for nuclei and inhomogeneous matter with a nuclear energy density functional*, *Phys. Rev. C* **107** (2023) 015802.
[15] G. Baym, C.J. Pethick, D. Pines and M. Ruderman, *Spin up in neutron stars: The future of the vela pulsar*, *Nature* **224** (1969) 872.
[16] P.W. Anderson and N. Itoh, *Pulsar glitches and restlessness as a hard superfluidity phenomenon*, *Nature* **256** (1975) 25.
[17] N. Andersson, K. Glampedakis, W.C.G. Ho and C.M. Espinoza, *Pulsar glitches: The crust is not enough*, *Phys. Rev. Lett.* **109** (2012) 241103.
[18] N. Chamel, *Crustal entrainment and pulsar glitches*, *Phys. Rev. Lett.* **110** (2013) 011101.
[19] N. Chamel, *Neutron conduction in the inner crust of a neutron star in the framework of the band theory of solids*, *Phys. Rev. C* **85** (2012) 035801.
[20] Y. Kashiwaba and T. Nakatsukasa, *Self-consistent band calculation of the slab phase in the neutron-star crust*, *Phys. Rev. C* **100** (2019) 035804.
[21] G. Watanabe and C.J. Pethick, *Superfluid density of neutrons in the inner crust of neutron stars: New life for pulsar glitch models*, *Phys. Rev. Lett.* **119** (2017) 062701.